PHYSICAL REVIEW E **96**, 042154 (2017)

Action at a distance in classical uniaxial ferromagnetic arrays

D. B. Abraham,[1] A. Maciołek,[2,3] A. Squarcini,[3,4,*] and O. Vasilyev[3,4]

[1]*Theoretical Physics, Department of Physics, University of Oxford, 1 Keble Road, Oxford OX1 3NP, United Kingdom*

[2]*Institute of Physical Chemistry, Polish Academy of Sciences, Kasprzaka 44/52, PL-01-224 Warsaw, Poland*

[3]*Max-Planck-Institut für Intelligente Systeme, Heisenbergstr. 3, D-70569 Stuttgart, Germany*

[4]*IV Institut für Theoretische Physik, Universität Stuttgart, Pfaffenwaldring 57, D-70569 Stuttgart, Germany*

(Received 30 June 2017; published 26 October 2017)

We examine in detail the theoretical foundations of striking long-range couplings emerging in arrays of fluid cells connected by narrow channels by using a lattice gas (Ising model) description of a system. We present a reexamination of the well known exact determination of the two-point correlation function along the edge of a channel using the transfer matrix technique and a different interpretation is provided. The explicit form of the correlation length is found to grow exponentially with the cross section of the channels at the bulk two-phase coexistence. The aforementioned result is recaptured by a refined version of the Fisher-Privman theory of first order phase transitions in which the Boltzmann factor for a domain wall is decorated with a contribution stemming from the point tension originated at its end points. The Boltzmann factor for a domain wall together with the point tension is then identified exactly thanks to two independent analytical techniques, providing a critical test of the Fisher-Privman theory. We then illustrate how to build up the network model from its elementary constituents, the cells and the channels. Moreover, we are able to extract the strength of the coupling between cells and express them in terms of the length and width and coarse-grained quantities such as surface and point tensions. We then support our theoretical investigation with a series of corroborating results based on Monte Carlo simulations. We illustrate how the long-range ordering occurs and how the latter is signaled by the thermodynamic quantities corresponding to both planar and three-dimensional Ising arrays.

DOI: 10.1103/PhysRevE.96.042154

I. INTRODUCTION

Recent experimental work by Gasparini *et al.* [1] has demonstrated striking action-at-a-distance effects in superfluid ^{4}He. The typical system is formed from a two-dimensional (2D) array of identical microscopic boxes etched in a Si wafer. These are filled with liquid ^{4}He and then coupled by pouring a relatively thin supernatant layer of liquid ^{4}He on top. Another technique for achieving coupling is to use a network of fluid channels [2]. The signature of action-at-a-distance is provided by accurate thermodynamic measurements, which show a quite unexpected "shoulder." The dimensions used in these experiments can be appreciated from Fig. 1.

A crucial factor in this phenomenology is the proximity induced by both the size and connectivity of the boxes, together with the nearness to the critical point. A precise discussion on the relevance of proximity effects on the enhancement of ordering in the context of the Gasparini *et al.* experiment can be found in [3]. Perron *et al.* [4] suggested that this class of experimental results might be a more widespread consequence of the critical phenomenon than previously supposed. Stimulated by these remarks, we have shown [5] that for Ising systems (an entirely different universality class), there is a divergent length scale (not the usual critical one) which is responsible for emergent long-ranged effects. This brings together ideas of Kac [6] on asymptotic spectral degeneracy in transfer matrices, the Fisher-Privman [7] theory of finite-size effects in first order phase transitions (and other systems), and the appropriate solution for the planar Ising model on a strip with free boundary conditions [8]. The latter shows first how effective the Fisher-Privman theory is when accurate input data are used. To provide this accurate input data, we give another exact solution, which gives as a bonus an exact result for the point tension but in a different context from [9]. Our thinking is illustrated and extended by some Monte Carlo simulations.

The layout of the paper is as follows: in Sec. II A we summarize the calculation of the pair correlation function [Eq. (22)] for spins located in the edges of the strip [8]. The algebra of the original derivation [8] is quite heavy, so we have focused here on the physical motivation, drawing analogies with the quantum mechanics of spinless fermions on a finite line (with ends, rather than the more transparent case with cyclic boundary conditions). Then, in Sec. II B, the same problem is treated in a completely different way using the Fisher-Privman theory [7]. We point out that introducing a hypothetical point tension in the statistical weight of an isolated domain wall gives precise agreement with part of the exact solution in Sec. II A. Normally, such contributions appear to be ignored but they are mandatory if critical scaling is to be captured. We also consider how an effective coupling is to be set up in a "network" lattice of boxes (each characterized by an up and down magnetization, which will be valid for large enough boxes). These "boxes" are coupled by strips in which the internal degrees of freedom have been summed out, producing an Ising superlattice of nodes which can display long-range order which, since the effective coupling is temperature dependent, is far from obvious.

After this, in Sec. III we derive the Fisher-Privman weight from first principles in an Ising strip and show that it has exactly the value deduced on phenomenological grounds. The fact that this can be done shows how good the Fisher-Privman theory is when an appropriate weight is used.

In Sec. IV we collect the results obtained by means of numerical simulations. This section contains 12 figures. The quantities of interest which are determined numerically are

*Corresponding author: squarcio@is.mpg.de

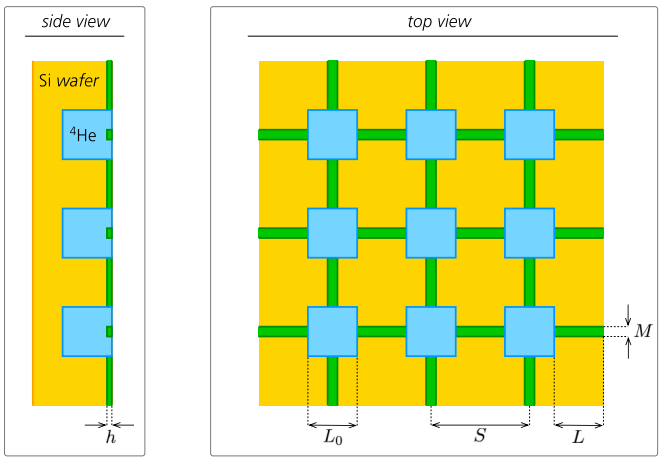

FIG. 1. The network of boxes from top view (right) and from side view (left). The typical dimensions considered in the experimental setup (see text) are $M \sim 1\ \mu$m, $L \sim 2\ \mu$m, $L_0 \sim 2\ \mu$m, $h \sim 30$ nm.

defined in Sec. IV A. Then, we present our results for one-dimensional (1D) arrays of squares (Sec. IV B) and 2D arrays of squares (Sec. IV C) connected by strips. The numerical determination of the effective coupling between boxes forming the array is showed in Sec. IV D and compared against the analytical prediction (30). We conclude the numerical part by showing the results for 2D arrays of cubes connected by channels (Sec. IV E).

Our final conclusive remarks are then summarized in Sec. V. The detailed calculations corresponding to Sec. III are collected in Appendix A. Then, we further discuss the Kac theory [6] of asymptotic degeneracy in transfer matrix spectra in Appendix B.

II. THEORY

A. Correlation function

We consider the correlation function between two spins in the edge of a planar Ising ferromagnet with zero magnetic field and strip geometry as shown in Fig. 2. The significance of having the spins in an edge is that this calculation is particularly tractable in the transfer matrix language [8] and its correct interpretation leads to a significant enhancement of the Fisher-Privman theory of finite-size effects [7]. The transfer matrix calculation builds up the lattice from column to column (see Fig. 2) with the operator

$$V_1 = (2\sinh 2K_1)^{M/2} \exp\left[-K_1^* \sum_{m=1}^{M} \sigma_m^z\right], \qquad (1)$$

where $\tanh K_1 = e^{-2K_1^*}$. Here, we are using the Schultz, Mattis, and Lieb [10] convention for spin operators σ_m^i, $i = x,y,z$, with *ordered* direction taken as x. The prefactor $(2\sinh 2K_1)^{M/2}$ will always cancel out with the normalizing partition function and thus we omit it for simplicity, as it will not report in the final answer. The transfer matrix V_2 which accounts for the interactions within columns is of the diagonal form

$$V_2 = \exp\left[K_2 \sum_{m=1}^{M-1} \sigma_m^x \sigma_{m+1}^x\right] \qquad (2)$$

for strip boundary conditions as in Fig. 2. The spectrum of the symmetrized product $V = V_2^{1/2} V_1 V_2^{1/2}$ was determined some time ago [8] by an amalgamation of the techniques of Kaufman [11] and of Schultz, Mattis, and Lieb (SML) [10]. It was Kaufman who made the essential step of introducing the Jordan-Wigner transformation [12], which reduces the rather intractable spin problem to one involving quadratic forms of spinors. Her method of diagonalization was made more tractable by SML, who drew an analogy with the pairing ideas of Anderson [13] and of Nambu [14]. Essentially, if one has a good working knowledge of the Bardeen, Cooper, and Schrieffer theory of superconductivity [15], then the Onsager theory [16] has been brought within the pabulum of any reasonably well-educated theoretical physicist.

The expression for the edge-spin pair correlation function is

$$C(n) = \langle \sigma_{1,1}\sigma_{1,n+1}\rangle = \langle \Phi|\sigma_1^x V^n \sigma_1^x|\Phi\rangle \Lambda_0^{-n}, \qquad (3)$$

where $|\Phi\rangle$ is the maximal eigenvector (unique by the Perron-Frobenius theorem [17]) with eigenvalue Λ_0. This result has been obtained by imposing periodic boundary

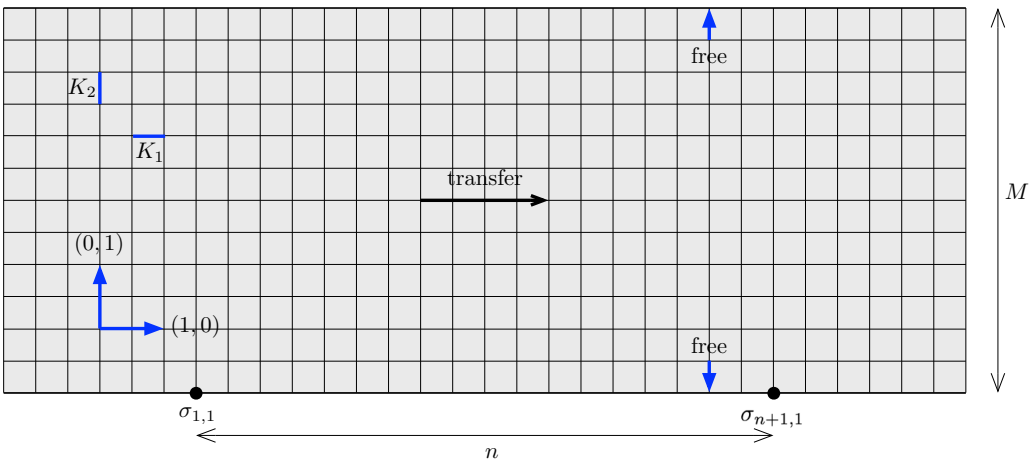

FIG. 2. Ising model on a planar lattice with free boundary conditions and nearest-neighbor interactions $K_j > 0$, $j = 1,2$, is shown. The transfer direction is indicated. In the applications considered here, we impose cyclic boundary conditions in the (1,0) direction.

conditions in the strip axial direction and then taking the limit of infinite strip length.

The Jordan-Wigner transformation, which is the crucial step introduced by Kaufman, as we stated above, is given by

$$f_m^\dagger = P_{m-1}\left(\sigma_m^x + i\sigma_m^y\right)/2, \quad 2 \leqslant m \leqslant M$$
$$\text{and} \quad f_1^\dagger = \left(\sigma_1^x + i\sigma_1^y\right)/2, \tag{4}$$

with the Jordan-Wigner tail or string being specified by

$$P_m = \prod_{j=1}^{m}\left(-\sigma_j^z\right) = i^m \exp\left[-i\sum_{j=1}^{m}\sigma_j^z\right]. \tag{5}$$

The Fermi field obeys the anticommutation relations $[f_m, f_n^\dagger]_+ = \delta_{mn}, [f_m, f_n]_+ = 0$. The connection of the operator P_M with spin rotations (inversions) in a column of a lattice is now obvious, as are the commutation relations

$$[V_1, P_M] = [V_2, P_M] = 0. \tag{6}$$

This implies that we can seek simultaneous eigenvectors of V and P_M. The V_j, $j = 1,2$, become quadratic forms in fermions:

$$V_1 = \exp\left[-K_1^*\sum_{m=1}^{M}(2f_m^\dagger f_m - 1)\right],$$
$$V_2 = \exp\left[K_2\sum_{m=1}^{M-1}(f_m^\dagger - f_m)(f_{m+1}^\dagger + f_{m+1})\right]. \tag{7}$$

The correlation function in (3) is expressed in terms of the Fermi fields as

$$C(n) = \langle\Phi|(f_1^\dagger + f_1)V^n(f_1^\dagger + f_1)|\Phi\rangle\Lambda_0^{-n}. \tag{8}$$

A consequence of taking the spins in the edge is the *linearity* of the forms representing the quantum mechanical treatment of spinless fermions on a finite line. We have hopping terms, which correspond to kinetic energy, and onsite energy terms. Thus, we anticipate left- and right-going waves characteristic of the bulk, which may be compared with the SML solution. The "in" and "out" waves at the left boundary must be matched to fit the boundary conditions; they become "out" and "in" waves at the right boundary, which must also be matched and made compatible with the left boundary. This generates the discretization condition for the fermion momentum. The only additional feature is that on the lattice there may be a local modification of amplitudes at the ends of the column. We find that

$$V = \exp\left\{-\sum_k \gamma(k)[X^\dagger(k)X(k) - 1/2]\right\}, \tag{9}$$

where $X(k)$ are the Fermi operators, details of which will follow, and $\gamma(k)$, the celebrated Onsager function [16], is that solution of

$$\cosh\gamma(k) = \cosh 2K_1^*\cosh 2K_2 - \sinh 2K_1^*\sinh 2K_2\cos k, \tag{10}$$

which is non-negative for real k. This requirement makes the vacuum for the operators also the maximal eigenvector: $X(k)|\Phi\rangle = 0$.

The discretization condition mentioned above for k is

$$e^{iMk} = s\,e^{i\delta^*(k)}, \quad s = \pm 1 \tag{11}$$

where s encodes reflection behavior [18,19] of the eigenvectors and the angle $\delta^*(k)$, also introduced by Onsager, is defined by

$$e^{i\delta^*(k)} = \left(\frac{B}{A}\right)^{1/2}\left[\frac{(e^{ik} - A)(e^{ik} - B^{-1})}{(e^{ik} - A^{-1})(e^{ik} - B)}\right]^{1/2}. \tag{12}$$

The location of the square-root branch points in the above is determined by

$$A = \exp(K_1 + K_2^*) \quad \text{and} \quad B = \exp(K_1 - K_2^*). \tag{13}$$

The choice of the branch for $\gamma(k)$ determines that in the discretization equation (12). For subcritical temperatures, we have $K_1 > K_2^* > 0$; thus, $A > B > 1$ and $\delta^*(0) = 0$ (mod 2π). It is convenient to define, as did Kaufman, the spinors by

$$\Gamma_{2m-1} = f_m^\dagger + f_m, \quad \Gamma_{2m} = -i(f_m^\dagger - f_m), \quad m = 1, \ldots, M. \tag{14}$$

These have a simple representation in terms of the $X(k)$ which is useful for calculating correlation functions; this is

$$\Gamma_m = \sum_k N(k)[y_m^*(k)X^\dagger(k) + y_m(k)X(k)], \tag{15}$$

where the normalization factor $N(k)$ is not needed in the computation and

$$y_{2m}(k) = iN(k)\sin mk, \quad y_{2m+1}(k) = N(k)\sin[km - \delta^*(k)],$$
$$m = 1, \ldots, M-1, \tag{16}$$

with the boundary values

$$y_1(k) = -N(k)\cosh K_2\sin\delta^*(k),$$
$$y_{2M} = -isN(k)\cosh K_2\sin\delta^*(k). \tag{17}$$

Here, we see the intuitive ideas above, between (8) and (9), in action. Taken with the discretization condition, (15), (16) and (17) guarantee

$$[X(k_1), X(k_2)] = 0, \quad [X(k_1), X^\dagger(k_2)] = \delta_{k_1,k_2}. \tag{18}$$

Notice that $k = 0$ and π generate trivial solutions and that, to avoid repetition and triviality, the momenta should satisfy $0 < k < \pi$.

In order to calculate the edge-pair correlation function, the first step is to determine the allowed momenta. This is an elementary matter using techniques from elementary calculus. If we consider zeros of $Mk - j\pi - \delta^*(k)$ for $A > B > 1$, there is one (in fact at least one) for each $j = 1, \ldots, M-1$. With $j = 0$, there is a nontrivial one if $M < d\delta^*(\omega)/d\omega|_{\omega=0}$ the slope of δ^* at $k = 0$ and when $M > d\delta^*(\omega)/d\omega|_{\omega=0}$, there is one with a pure imaginary wave number with $s = +1$. Thus, $k = iv$, v real and

$$e^{-Mv} = s\,e^{i\delta^*(iv)}. \tag{19}$$

It is then a straightforward matter to show there is such a solution for $s = +1$, $0 < v < \hat{\gamma}(0), \hat{\gamma}(0) = 2(K_1 - K_2^*)$, but only if $M > d\delta^*(\omega)/d\omega|_{\omega=0}$; note that $\hat{\gamma}(k)$ is just $\gamma(k)$ with

K_1 and K_2 interchanged. It is easy to see that

$$v = \hat{\gamma}(0) - 2(\sinh 2K_1 \sinh 2K_2)^{-1} \sinh \hat{\gamma}(0)\, e^{-2M\hat{\gamma}(0)} + O(e^{-4M\hat{\gamma}(0)}), \tag{20}$$

and that

$$\gamma(iv) = 2 \sinh 2K_1^* \sinh \hat{\gamma}(0)\, e^{-M\hat{\gamma}(0)} + O(e^{-2M\hat{\gamma}(0)}). \tag{21}$$

Thus, we have found an asymptotic degeneracy in the spectrum (see Appendix B) and this is associated with a surface mode in which the eigenfunctions decay away from the surface on a scale of $\xi_b = 1/\hat{\gamma}(0)$; this is the bulk correlation length, up to the Kadanoff-Wu anomaly [20]. The edge-spin pair correlation function comes out in the form

$$C(n) = m_e^2 \exp[-2n \sinh 2K_1^* \sinh \hat{\gamma}(0)\, e^{-M\hat{\gamma}(0)}] + \sum_k |y_1(k)|^2 \exp[-n\gamma(k)]. \tag{22}$$

The first term above decays to zero on a new, emergent, length scale $\propto [\sinh \hat{\gamma}(0)]^{-1} e^{M\hat{\gamma}(0)}$ on which long-ranged order is ultimately lost. It also displays a scaled form in the vicinity of the bulk correlation length, that is the bulk scaling limit. In the above,

$$m_e = \sqrt{\frac{B - B^{-1}}{B - A^{-1}}} \tag{23}$$

is the edge spontaneous magnetization, as originally determined by McCoy and Wu [21]. The second term on the right-hand side is bounded above by $\exp[-n\gamma(0)]$; this gives a clear separation of length scales.

B. Fisher-Privman theory applied to the strip

Any configuration of the spins on the Ising strip with free boundary conditions can be analyzed to extract arrangements of domain walls going from side to side of the strip; these walls separate oppositely magnetized domains which are themselves reasonable approximations to bulk strip states for M large enough. We may consider that fluctuation effects with a spatial extent of about the bulk correlation length or less have been summed over, a coarse graining producing a mesoscale model (at least in principle). In this case, the space between domain walls is essentially featureless, having a spatially averaged magnetization of bulk spontaneous magnetization, denoted m^*; see Fig. 3.

The energy of any domain wall should be replaced by a coarse-grained fluctuation free energy of Helmholtz type. Following Fisher and Privman [7], we can go one step further and regard the domain walls as point particles in a quasi-one-dimensional system, the equilibrium statistical mechanics of which can be determined exactly in a suitable approximation. Let the statistical weight of any domain wall in isolation be denoted by $\tilde{w}$. Then, the two spins in the strip separated by n lattice spacings will be parallel (resp. antiparallel) if the number of domain walls in the interviewing space are even (resp. odd). The correlation function of these spins, denoted $\mathcal{C}(n)$, is given by

$$\begin{aligned}\mathcal{C}(n) &= \left\{\tfrac{1}{2}[(1+\tilde{w})^n + (1-\tilde{w})^n] \right. \\ &\quad \left. - \tfrac{1}{2}[(1+\tilde{w})^n - (1-\tilde{w})^n]\right\} \big/ (1+\tilde{w})^n \\ &= [(1-\tilde{w})/(1+\tilde{w})]^n. \end{aligned} \tag{24}$$

Here, we assume the domain walls have negligible interactions. Evidently, we have

$$\begin{aligned}&\mathcal{C}(n) = e^{-n\lambda(\tilde{w})}, \\ &\lambda(\tilde{w}) = \ln[(1+\tilde{w})/(1-\tilde{w})] = 2[\tilde{w} + 3^{-1}\tilde{w}^3 + O(\tilde{w}^5)].\end{aligned} \tag{25}$$

Thus, for small $\tilde{w}$, where the theory is likely to be particularly pertinent, we have $\lambda(\tilde{w}) \simeq 2\tilde{w}$. The usual practice is to write

$$\tilde{w} = e^{-M\tau} \tag{26}$$

for a strip of width M, where τ is the surface tension, a coarse-grained entity as we would expect; this is precisely what one would normally do in Helmholtz fluctuation theory. This does not agree with (22), which is the exact solution for the edge-pair function. It would agree, were $\tilde{w}$ to be replaced by w, where

$$w = \sinh 2K_1^* \sinh \hat{\gamma}(0)\, e^{-M\hat{\gamma}(0)}. \tag{27}$$

Since $\hat{\gamma}(0) = \tau$, where τ is the surface tension for an interface oriented at right angles to the strip axis, we recapture (22) from (25) above in the linear regime. Another more phenomenological angle is to note that the Fisher-Privman result above does not scale, but it would do so, were we to write

$$w = a\, \xi_b^{-1} e^{-M\tau}, \tag{28}$$

where ξ_b is the bulk correlation length, related precisely to τ by the relation $\tau\xi_b = \frac{1}{2}$, which is valid for all temperatures and is an application of duality [22,23]. It is also compatible with Widom scaling [24]. As it stands, if all we demanded was scaling rather than agreement with (22), then the parameter a in (28) would be an arbitrary scale factor. In Appendix A, we will calculate w by another exact solution for the Ising strip and see that it is precisely of the form of (27). Also, we should think of the prefactor, which converts (26) to (27), as arising from point tension contributions of magnitude τ_p. In other words, we can write $w = e^{-2\tau_p - M\tau}$ and single out the factor a/ξ_b as the one due to the point tension. The incorporation of the point tension in the Boltzmann weight defines the enhanced Fisher-Privman theory, but it might just as well be said to be Fisher-Privman theory properly carried out.

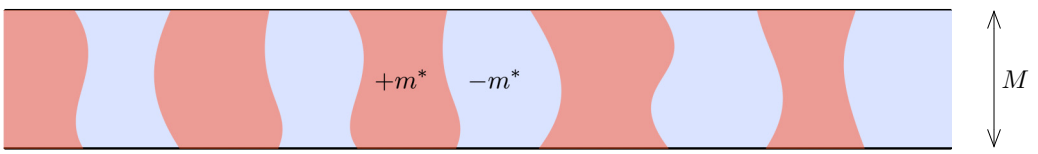

FIG. 3. A schematic representation of a typical domain wall configuration on the Ising strip. Typically, the domains are widely separated along (1,0) and thus infrequent.

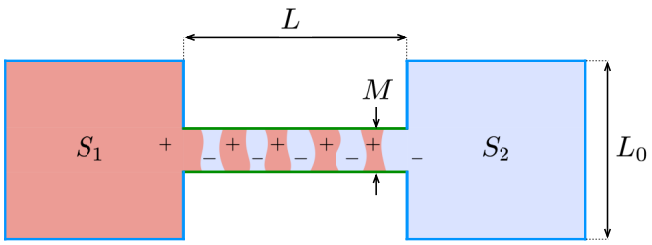

FIG. 4. Side view of an Ising system comprised of two cubic lattice boxes of a side L_0 connected by a $L \times M$ strip with $L \gg M$. We assume $L_0 \gg M$.

With M fixed, w may ultimately be reduced by going towards the critical point. This is contrary to the usual intuition about such matters and it enhances the domain of validity of the Fisher-Privman theory in an interesting way; see in particular, the discussion above (34). Finally, we discuss scaling. If we take the scaling limit $M \to \infty$, $\tau \to 0$, $M\tau \to \overline{M}$, $n\tau \to \overline{n}$, we see that the nonlinear terms in (25) generate corrections to scaling. For simplicity, take the isotropic lattice with $K_1 = K_2$, so that $\sinh 2K_1^* = 1$ at $\tau = 0$. Then, we have

$$\mathcal{C}(n) = \exp[-2\overline{n}e^{-\overline{M}}] + O(\tau^2). \tag{29}$$

Terms of higher order in $e^{-\overline{M}}$ have been neglected in this equation since, for consistency, we would have to consider higher order terms in (21).

We now consider network models of hypercubic coupled "boxes." Each one is a finite Ising lattice in d dimensions, with $d = 2,3$ and side L_0. The interactions in the box and L_0 are chosen to ensure that each such box contains essentially a single magnetic domain. Multiple domains, associated with domain walls that intersect the boundary of the box, are suppressed by a strictly positive surface tension (chosen large enough) and the extent of such a domain wall $\sim L_0^{d-1}$. Thus, any such box j has an average magnetization $m_0^* S_j$ where $S_j = \pm 1$ is an indicator variable and m_0^* approximates the spontaneous magnetization in d dimensions as $L_0 \to \infty$. In order to investigate coupling within this network, let boxes i and j be connected by a strip or rod of Ising type (see Fig. 4).

Then, if $S_i S_j = +1$ (resp. -1), there is an even (resp. odd) number of domain walls within the connector; these are treated by Fisher-Privman theory. The result is to generate a Boltzmann factor $A\, e^{K_{\rm eff} S_i S_j}$ where the parameter A will be of no further interest, but $e^{2K_{\rm eff}} = [(1+w)^L + (1-w)^L]/[(1+w)^L - (1-w)^L]$, where L is the strip length and w is the *a priori* weight of any domain wall, dependent as we have seen on the strip width M and the surface tension τ, as in (28). Introducing the variable $t = (1-w)/(1+w)$ this has the form

$$e^{2K_{\rm eff}} = (1+t^L)/(1-t^L), \tag{30}$$

with w given by Eq. (38) for $K_1 = K_2 \equiv K$, $N \to M$ and $\gamma(0) \to \tau$, hence,

$$w = (\sinh 2K)^{-1} \sinh \tau\, e^{-M\tau}\,. \tag{31}$$

It is crucial to note that $K_{\rm eff}$ is an effective Ising coupling which depends in a quite subtle way on M, τ, and K (the spin coupling within the strip).

Let us now consider the planar array of square boxes connected by one-dimensional Ising rods. Thus, it is an interesting question whether the network can display long-range order. This would be so if $e^{2K_{\rm eff}}$ can be chosen to exceed the critical value of $1+\sqrt{2}$ of the $d = 2$ Ising model. Thus, the equation

$$1 + t^{L_c} = (1+\sqrt{2})(1 - t^{L_c}) \tag{32}$$

implies a critical surface $L_c(\tau, M)$, shown in Fig. 5(a). For $L < L_c$ (resp. $L > L_c$), the network is ordered (resp. disordered). Introducing scaling variables τL_c and $e^{-M\tau}$ the network

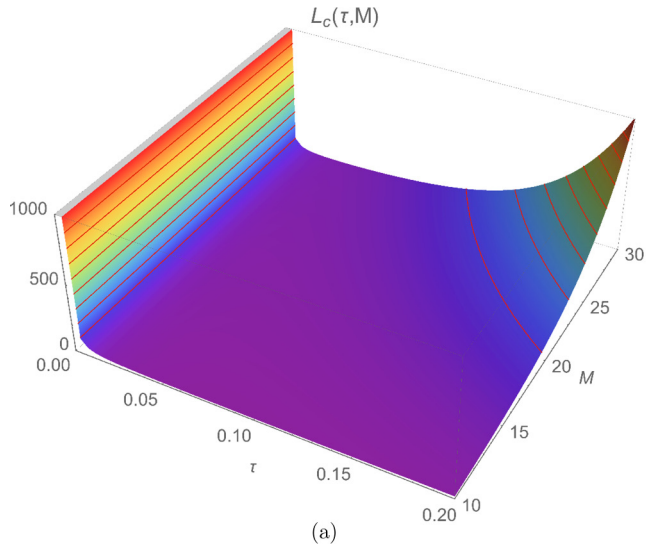

(a)

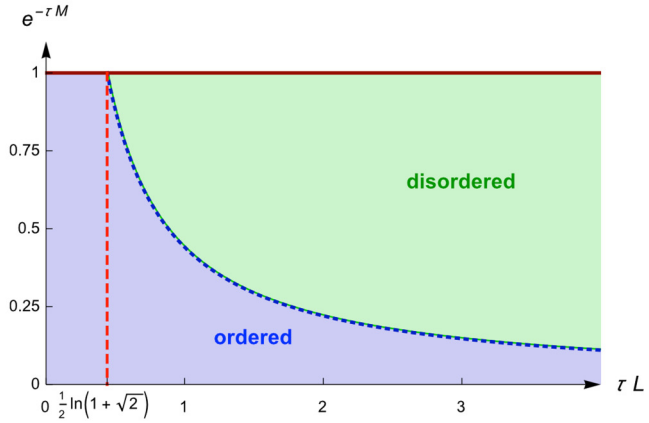

(b)

FIG. 5. (a) The critical length L_c as a function of the surface tension τ and the strip width M. Given τ and M, a system with a length smaller than L_c is ordered and corresponds to a point in the phase diagram below the surface of the graph. The iso-L_c contour lines are highlighted in red. Note the existence, for a given M, of ordered configurations for a pair of values of τ (reentrant phenomenon). (b) The phase diagram in terms of the scaling variables τL and $e^{-\tau M}$. The critical line $\tau L_c e^{-\tau M} = 2^{-1}\ln(1+\sqrt{2})$ separates ordered and disordered configurations, as illustrated in the shadowed regions. Notice that $e^{-\tau M}$ is bounded from above by unity since τ is non-negative.

critical point satisfies

$$\tau L_c\, e^{-M\tau} = 2^{-1}\ln(1+\sqrt{2}). \tag{33}$$

Thus, if $\tau L_c < 2^{-1}\ln(1+\sqrt{2})$, no such critical point is possible. This is shown in Fig. 5(b).

The role played by the point tension and the domain of validity of the refined Fisher-Privman theory can be neatly appreciated with the following considerations. Comparing the contribution of the imaginary wave number mode in the exact Ising strip calculation [Eq. (22)] and the result of the refined Fisher Privman model [Eq. (25) with $\tilde{w}$ replaced by w given by (31)], we should require for perfect matching that

$$\frac{1-w}{1+w} = \exp\{-\gamma[iv(M)]\}, \tag{34}$$

or $w = \tanh\{\gamma[iv(M)]/2\}$. Now, if we take the exact calculation of the weight, we get $w = \gamma[iv(M)]/2$, which agrees precisely to first order in $\gamma[iv(M)] \to 0$. The Fisher-Privman model neglects interactions between domain walls, other than a simple exclusion (walls cannot cross). This cannot be precisely correct. Now, examine $\gamma[iv(M)]$ given by (21) with $\hat{\gamma}(0) = \tau$,

$$\gamma[iv(M)] = 2\sinh 2K_1^*\sinh\tau\, e^{-M\tau} + O(e^{-2M\tau}), \tag{35}$$

just considering the first term, the behavior as a function of τ with M fixed implies investigating the function $\varphi(\tau) = \sinh\tau\, e^{-M\tau}$. Now, $\varphi(0) = 0$, which is a consequence of the line tension ($e^{-\tau_p} \propto \sinh\tau$). On the other hand, for $M \geqslant 2$, we have $\lim_{\tau\to\infty}\varphi(\tau) = 0$. Hence, there is a maximum when $\coth\tau_m = M$ or, equivalently, $\sinh\tau_m = (M^2-1)^{-1/2}$. After some algebra, we find that the maximum value of $\varphi(\tau)$ is

$$\varphi(\tau_m) = \frac{(M-1)^{\frac{M-1}{2}}}{(M+1)^{\frac{M+1}{2}}} = \frac{1}{Me}\left[1+O\left(\frac{1}{M}\right)\right]. \tag{36}$$

It is evident that the above can be made as small as one likes by taking M big enough. Consequently, the corresponding weight will be *small even for* $\tau \to 0$ *thanks to the point tension*; notice that this would not have been the case without the point tension contribution which would have made $w = O(1)$ in that precise limit. It follows that the refined Fisher-Privman approach is considerably more useful than one might have suspected.

III. EXACT BOLTZMANN WEIGHT AND POINT TENSION

As already stressed in Sec. II, the phenomenological Boltzmann weight for a domain wall given by (26) is not correct. Thus, by constructing the edge spin-spin correlation function in the manner of Fisher-Privman and matching it with the exact result (22) we deduced the exact Boltzmann weight given by (27). In this section, we further support the above identification by means of another exact, and independent, calculation. The idea is to determine the free energy associated with a domain wall running perpendicularly to the edges of the strip.

Following earlier definitions, if the strip with free edges (no magnetic fields) is wrapped onto a cylinder, as required by cyclic boundary conditions, then a *single* interface in the $(0,1)$ direction can be introduced by reversing a contiguous line of bonds as shown in Fig. 6. This statement is not quite correct: for sufficiently large M the line of defect bonds admits an *odd* number of interfaces, strictly speaking. For temperatures

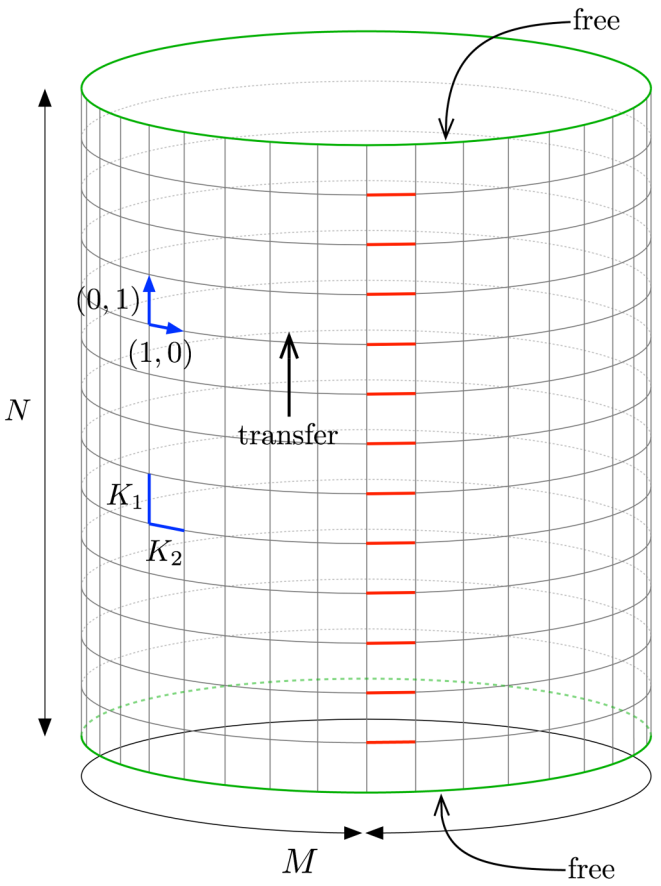

FIG. 6. Cylindrical lattice with a line of reversed bonds.

below the critical value for the bulk lattice, an incipient ordered state is expected, so provided the circumference is not too large, in a way that will be made precise in due course, there is a single magnetized phase having average magnetization approximately the bulk spontaneous value. Introducing a line of reversed bonds as shown in Fig. 6 will then indeed model an interface. The reader may like to note that this is not unlike the model of an interface from which Onsager extracted the first exact result for the surface tension [16].[1]

The computation of the excess free energy corresponding to the insertion of a line of reversed bonds boils down to determination of the ratio $Z^\times/Z$, where $Z^\times$ is the partition function of the cylindrical lattice with the line of reversed bonds and Z without such a line. Since the detailed computation of $Z^\times/Z$ is rather mathematical, we report here the final result, and refer to Appendix A for two exhaustive and detailed derivations. The result is

$$\frac{Z^\times}{Z} = M\sinh 2K_2^*\sinh\gamma(0)\, e^{-N\gamma(0)} + O(e^{-2N\gamma(0)}). \tag{37}$$

This is very satisfactory since with the cyclic boundary conditions as indicated there are M precisely equivalent translates of any configuration, hence the factor M which

[1]The detailed examination of the finite-size effects given here is, to the best of our knowledge, not yet reported in the literature.

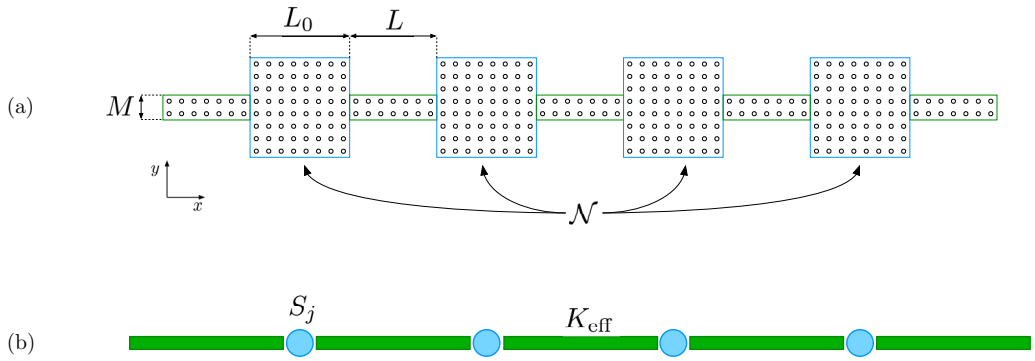

FIG. 7. (a) Geometry of a 1D array of $\mathcal{N}$ squares of size L_0 connected by strips (channels) of length L and width M. (b) The equivalent 1D system, that consists of $\mathcal{N}$ coarse-grained spin variables S_j connected by bonds with effective interaction $K_{\rm eff}$.

gives a Boltzmann entropy $\ln M$ in units of k_BT. The correct Boltzmann weight for a domain wall is thus

$$w = \sinh 2K_2^* \sinh\gamma(0) e^{-N\gamma(0)}, \tag{38}$$

which coincides with (27) under the exchange $K_1 \leftrightarrow K_2$ and $M \leftrightarrow N$, as it appears evident from the structure of the lattices of Figs. 2 and 6; note that under the first of the above replacements $\gamma(\omega) \leftrightarrow \hat{\gamma}(\omega)$. The exact Boltzmann weight (38) contains a surface tension contribution $\gamma(0)$, which agrees with Onsager [16], and a positive point tension[2] (the $d = 2$ analog of line tension in $d = 3$) having the value τ_p, where

$$\tau_p = -2^{-1} \ln[\sinh 2K_2^* \sinh\tau]. \tag{39}$$

The positiveness of τ_p follows from the fact that $0 < \sinh 2K_2^* \sinh\tau < 1$ for any subcritical temperature; see the end of Appendix A for the proof of this statement. We further note that while τ is a monotonically decreasing function of the reduced temperature, which eventually vanishes at the bulk critical point, the point tension is instead a monotonically increasing function of the reduced temperature with a logarithmic divergence at the bulk critical point.

IV. NUMERICAL SIMULATIONS

In order to test our predictions based on the extended Fisher-Privman theory [7] we have performed a series of Monte Carlo simulations of the Ising model.

A. Numerical method and observables

We consider the Ising model on a square lattice in two dimensions (2D) and on a simple cubic lattice in three dimensions (3D) with the lattice spacing $\ell = 1$ defined via the Hamiltonian

$$H = -J \sum_{\{(i,j),(i',j')\}} \sigma_{i,j}\sigma_{i',j'}, \tag{40}$$

where $\sigma_{i,j} = \pm 1$ denotes the spin variable. The parameter J, which we set equal to 1, is the spin-spin coupling constant and the sum $\{(i,j),(i',j')\}$ is taken over all nearest-neighbor pairs of sites (i,j) and (i',j') on the lattice. The total number of spins of the lattice is given by N_s. We shall consider different geometries, which will be specified later. For all geometries we assume open boundary conditions (OBC) in which the spins are free at the boundaries. For the square lattice, the critical value of the coupling constant $K = \beta J$, where $\beta = 1/(k_BT)$, is given by $K_c = (1/2)\ln(1+\sqrt{2}) \approx 0.440\,687$ [16]. Various estimations are available for $D = 3$ [25]; $K_c(D=3) \approx 0.221\,654\,4(3) \approx K_c(D=2)/2$.

We perform numerical simulation using a hybrid algorithm. One Monte Carlo step consists of one update of Wolff cluster and $N_s/4$ Metropolis updates of randomly selected spins. The Wolff cluster algorithm provides simultaneous flips of the entire squares and cubes and thus the faster relaxation in the vicinity of the critical point while Metropolis single spin algorithm provides higher efficiency in the low temperature region. We use standard definitions [26,27] for the thermodynamic quantities: the magnetization per spin is

$$m = \frac{1}{N_s}\left\langle \left| \sum_{\{(i,j)\}} \sigma_{i,j} \right| \right\rangle = \frac{1}{N_s}\langle M\rangle, \tag{41}$$

where the sum $\{(i,j)\}$ is taken over all spins of the system, the energy per spin is given by

$$e = -\frac{1}{N_s}\left\langle \sum_{\{(i,j),(i',j')\}} \sigma_{i,j}\sigma_{i',j'} \right\rangle = \frac{1}{N_s}\langle E\rangle, \tag{42}$$

the heat capacity is

$$C = \beta^2(\langle E^2\rangle - \langle E\rangle^2)/N_s, \tag{43}$$

and the magnetic susceptibility is

$$\chi = \beta(\langle M^2\rangle - \langle M\rangle^2)/N_s\,, \tag{44}$$

where $\langle E^2\rangle = \langle(\sum_{\{(i,j),(i',j')\}} \sigma_{i,j}\sigma_{i',j'})^2\rangle$ and $\langle M^2\rangle = \langle(\sum_{\{(i,j)\}} \sigma_{i,j})^2\rangle$. In the above definitions $\langle\ldots\rangle$ denotes the thermodynamic average over system states.

B. 1D array of squares

Our lattice network model of hypercubic Ising boxes connected by Ising strips (see Appendix A) does not exhibit

[2]The excess free energy (in k_BT units) takes the form $\mathcal{F} = -\ln M + N\gamma(0) - \ln[\sinh 2K_2^* \sinh\tau]$. The first term $-\ln M$ is an entropic contribution due to the fact that we can locate the domain wall in M positions which are equivalent under translation invariance, $N\hat{\gamma}(0)$ is the energy cost of an unpinned domain wall, $\tau_p = -2^{-1}\ln[\sinh 2K_2^* \sinh\tau]$ is the point tension originated at each anchoring point.

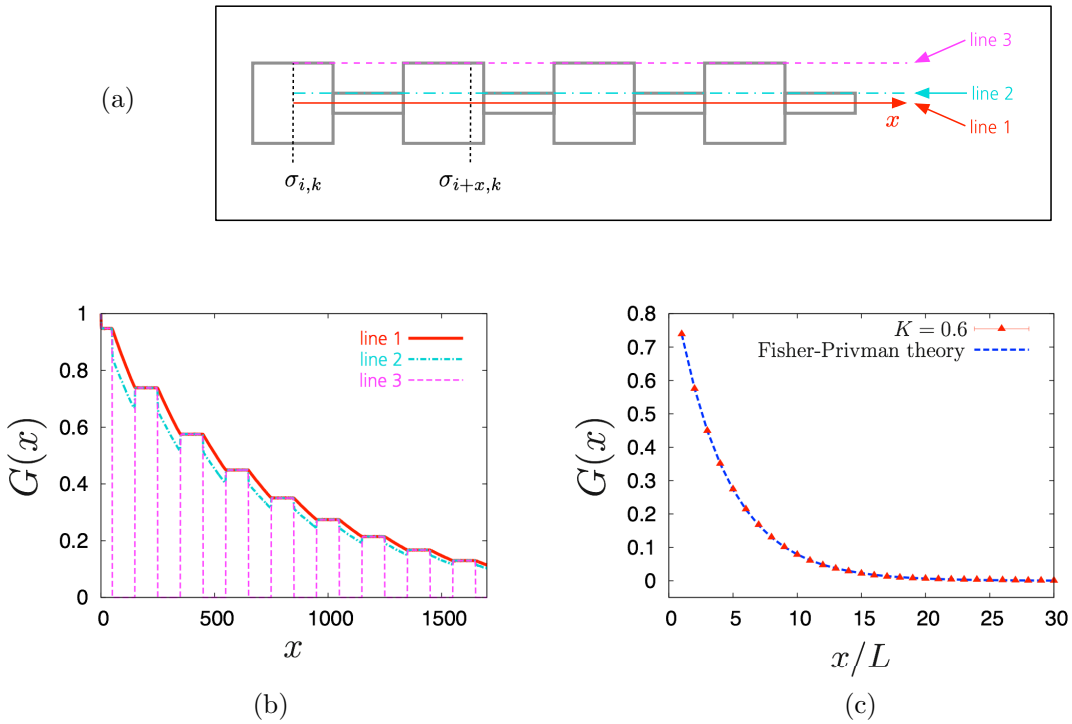

FIG. 8. (a) The scheme for the computation of the spin-spin correlation function $G(x)$ along three different lines: line 1 at the middle of the channel (red solid line), line 2 at the side of the channel (cyan dashed-dotted line), and line 3 at the side of the square (magenta dashed line). (b) Spin-spin correlation function $G(x)$ for the 1D array of $\mathcal{N} = 100$ squares of a side length $L_0 = 100$ as a function of the distance x along the three lines: the line passing through center of the channel (red solid line), through the side of the channel (cyan dashed-dotted line) and through the side of the square (magenta dashed line) for $K = 0.6$; the channel length is $L = 100$ and the width is $M = 10$. (c) The plateau values of $G(x)$ computed along the middle line of the channel as a function of x/L (symbols) follow the 1D Ising correlation function law given by Eq. (45) (dashed blue line) with $m_0^* = 0.97$.

a phase transition in one dimension. For the 1D network, however, we can use the exact form for the correlation function $G(x) = \langle S_i S_j \rangle$ between the boxes S_i and S_j, separated by x/L sites of the effective lattice with $x = i - j$; the latter reads as

$$G(x) \simeq (m_0^*)^2 (\tanh K_{\text{eff}})^{|x/L|}, \tag{45}$$

where K_{eff} is the effective coupling interaction, which from (30) admits the neat expression $\tanh K_{\text{eff}} = t^L$. In order to test this prediction, we take the system that consists of $\mathcal{N}$ squares of the size $L_0 \times L_0$ (each square contains L_0^2 spins) connected by strips of the length L and width M (the number of spins in the strip is equal to $L \times M$) [see Fig. 7(a)]. The system is periodic in the x direction; the first and the $\mathcal{N}$th squares are connected forming a ring. The total number of spins in the system is $N_s = \mathcal{N}(L_0^2 + LM)$. We have performed Monte Carlo simulations for the system of $\mathcal{N} = 100$ squares of size $L_0 = 100$ connected by channels of length $L = 100$ and various widths $M = 4,6,10,20,30,40$.

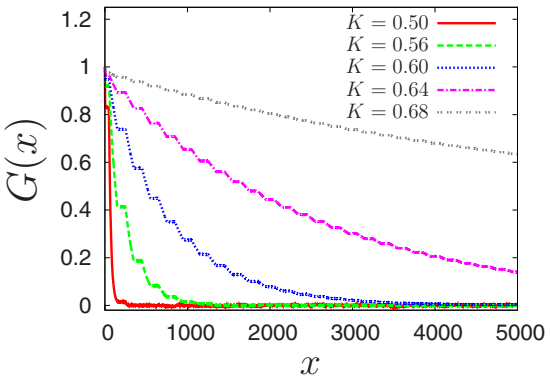

FIG. 9. Spin-spin correlation function $G(x)$ along the centers of the squares (line 1) as a function of the distance x for the same system as in Fig. 8 and various couplings, $K = 0.5,0.56,0.6,0.64,0.68$.

The spin-spin correlation function $G(x) = \langle \sigma_{i,k} \sigma_{i+x,k} \rangle$ is computed in the x direction along three different lines, as shown in Fig. 8(a). The horizontal coordinate $x = 0$ of the first spin $\sigma(0)$ is always at the center of the square box. For the vertical coordinate y of both spins we consider three cases: the centers of the squares, the sides of the channels, and the sides of the squares, denoted, respectively, with the lines 1, 2, and 3 of Fig. 8(a). Let us note that the correlations along the edges of the squares exist only if the second spin $\sigma(x)$ is located within a square.

In Fig. 8(b) we plot the spin-spin correlation function along these lines for a channel of width $M = 10$ and for the coupling $K = 0.6$. One can see that $G(x)$ stays constant within the squares and depends only on the mutual distance between the latter, which supports the crucial assumption for derivations in Appendix A that the boxes are ordered. Figure 8(c) shows the values of plateaux from Fig. 8(b) plotted as function of

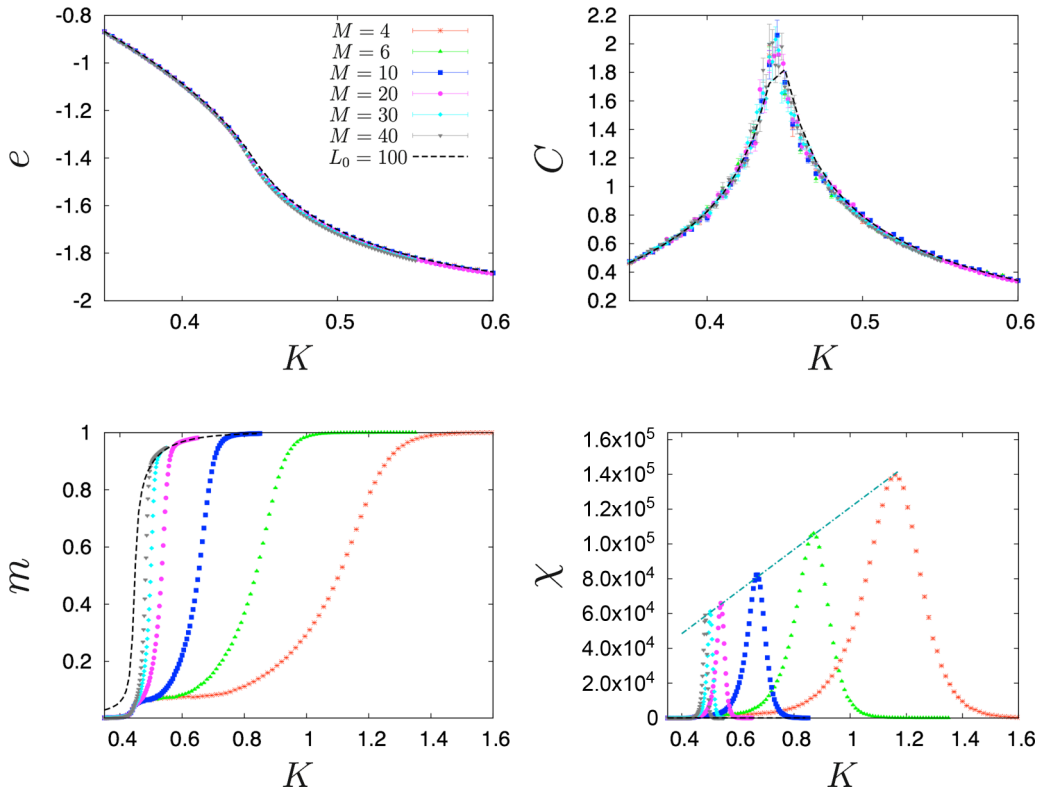

FIG. 10. Thermodynamic quantities for a 1D array of $\mathcal{N} = 100$ squares of size $L_0 = 100$ connected (in a periodic way) by strips of size $100 \times M$ as a function of the coupling K: energy per spin e (upper panel, left), heat capacity C (upper panel, right), magnetization per spin m (lower panel, left), and magnetic susceptibility χ (lower panel, right). Results for a single OBC square with $L_0 = 100$ are plotted by black dashed line for comparison (except for the plot of χ).

x/L together with the theoretical prediction given by Eq. (45). Perfect agreement is obtained for $m_0^* = 0.97$ corresponding to the spontaneous magnetization at $K = 0.6$.

In Fig. 9 we plot $G(x)$ for the same system as in Fig. 8 for several values of the coupling constant K. We can see that already for $K = 0.5$ the spins within the first square are correlated. Note that $G(x) > 0.8$ for $x < 50$. The spatial extent of the correlations grows by increasing the coupling K and, ultimately, the correlations spread across the whole system by further increasing of K. This feature can be linked to

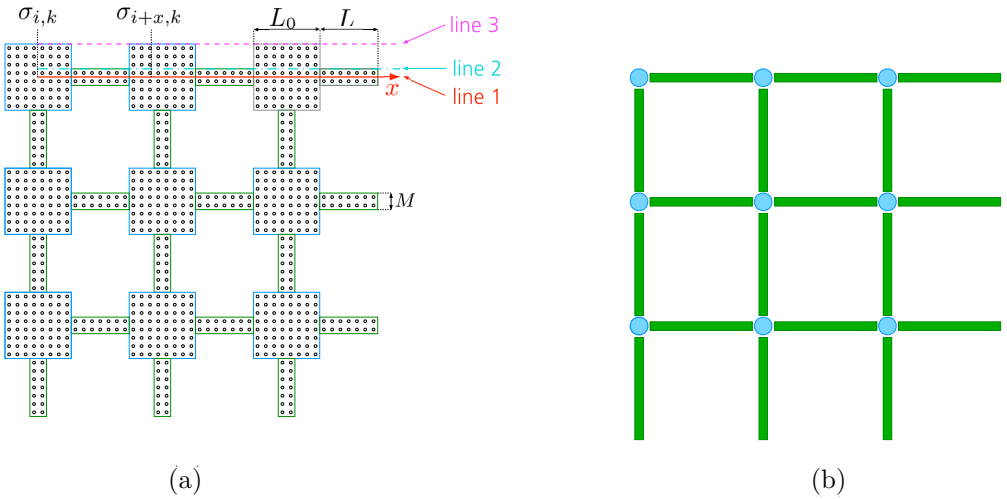

FIG. 11. (a) Geometry of a 2D array of a linear size $\mathcal{N}$ consisting of $\mathcal{N}^2$ squares of size L_0 connected by strips (channels) of the length L and the width M. The scheme for computation of the spin-spin correlation function $G(x) = \langle \sigma(0)\sigma(x) \rangle$ for three different lines: line 1 at the middle of the channel (red solid line), line 2 at the side of the channel (cyan dashed-dotted line), and line 3 at the side of the square (magenta dashed line). (b) Geometry of the equivalent network model.

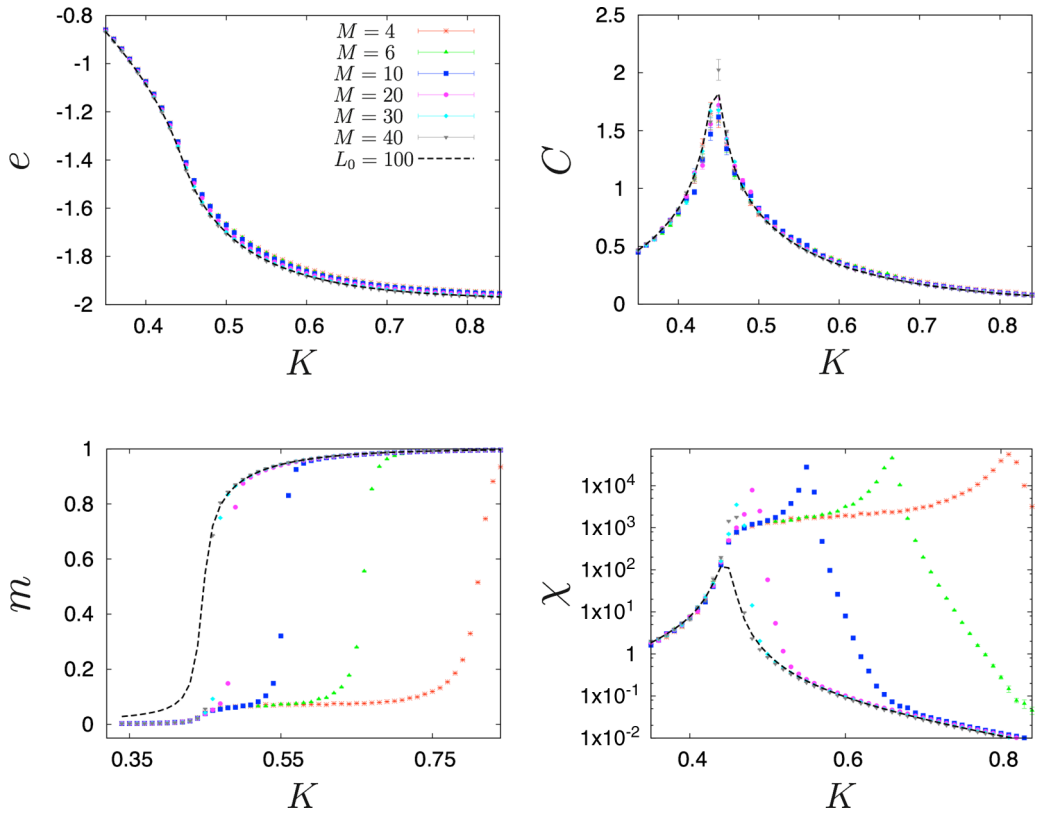

FIG. 12. Thermodynamic quantities for the system shown in Fig. 11 with $\mathcal{N} = 10$ and $L_0 = 100$ connected (in a periodic way) by strips of size $100 \times M$ as a function of the coupling K: energy per spin (upper panel, left) e, heat capacity C (upper panel, right), magnetization per spin m (lower panel, left), and magnetic susceptibility χ (lower panel, right). Results for a single OBC square $L_0 = 100$ are plotted with a black dashed line for comparison.

the behavior of thermodynamic quantities as functions of K, which is presented in Fig. 10.

For comparison, we plot in this figure also the results for the single OBC square of the size $L_0 = 100$ (black dashed line). One can see that for the studied system sizes, the energy-related quantities such as the energy per spin e and the heat capacity for the single square and for the 1D array of coupled squares are almost identical; see Figs. 10(a) and 10(b). The peak in the heat capacity of a single PBC square indicates the rounded 2D continuous order-disorder phase transition. In contrast, the magnetization-related quantities such as the magnetization per spin m and the magnetic susceptibility exhibit a rounded transition at a value of $K_c(M) > 0.45$, which for this coupled system depends on the width of connecting channel M; see Figs. 10(c) and 10(d). The dashed-dotted line in Fig. 10(d) shows that the location of this rounded transition, as indicated by the maximum of the susceptibility $\chi_{\max}$, grows linearly with K as the width of the channel M is decreased. For the system

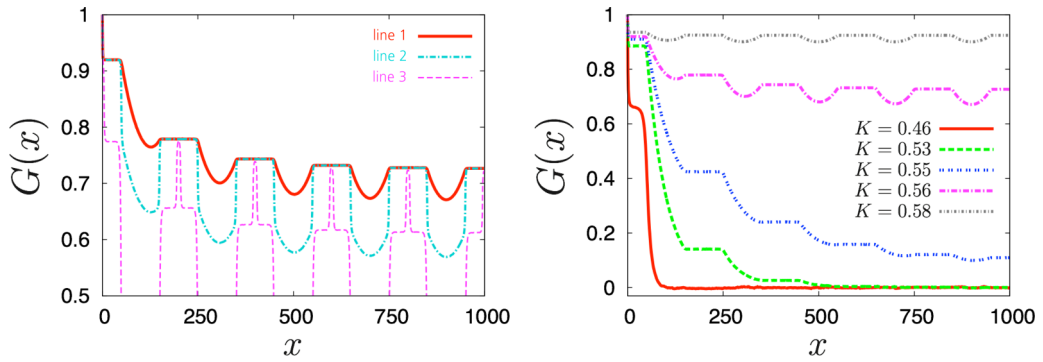

FIG. 13. Left panel: the spin-spin correlation function $G(x)$ as a function of the distance x for a system with $L_0 = 100$, $L = 100$, $M = 10$ for $K = 0.56$ along the three different lines: centers of the channels (red solid line), sides of the channels (cyan dashed-dotted line), and along the sides of the squares (magenta dashed line). Right panel: the correlation function along the centers of the channels for various couplings $K = 0.46, 0.53, 0.55, 0.56, 0.58$.

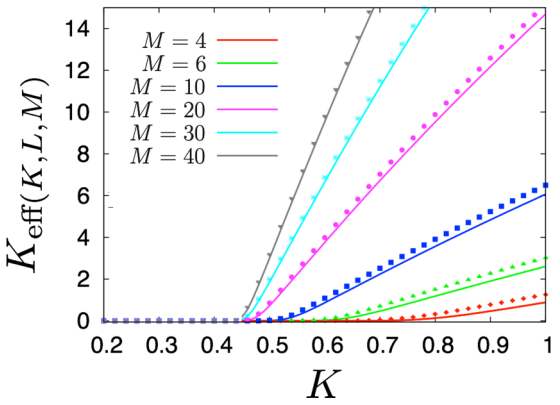

FIG. 14. The effective interaction constant $K_{\rm eff}$ mediated by the Ising strip (channel) of the size $L \times M$ as a function of K for $L = 100$ and $M = 4,6,10,20,30,40$. Lines correspond to Eq. (30), symbols correspond to the MC results (48).

of Fig. 9, i.e., for $M = 10$, the maximum of the magnetic susceptibility χ occurs at $K \approx 0.66$. Around this maximum the spins in the whole 1D array become correlated as can be inferred from the behavior of $G(x)$ shown in this figure. This is a manifestation of finite-size effects on the order-disorder transition in 2D systems [28]. The (pseudo)critical coupling is shifted to the higher values of K with respect to $K_c(D = 2) \approx 0.440\,687$ of the bulk 2D Ising model, this shift depends both on the geometry and the size of the system.

We have checked how the size of constituents of the array influences both the heat capacity and the magnetic susceptibility. We have found that enlarging the connecting volumes leads to the increase of the maximum of the heat capacity, while the location of the peak remains practically unchanged. We observe that making the connecting channel shorter does not influence the heat capacity C. On contrary, the peak of the susceptibility becomes only slightly larger for larger boxes, but shortening the channel length leads to the shift of the peak of χ to regions of smaller K.

From Fig. 10 we can conclude that the rounded ordering transition in the array of coupled volumes occurs in two stages. At the first stage, spins in every square become ordered, this process takes place about the (pseudo)critical point $K_{c,L_0} \simeq 0.45$ for an isolated OBC square of size L_0 and does not depend on the geometry of the connecting channels. This first stage is responsible for the peak of the heat capacity. This rounded phase transition corresponds to a system with the same spatial dimension (and universality class) as the coupled volumes; for the case at Hand, the volumes are actually two-dimensional entities. However, right at this transition point different squares stay uncorrelated. As we increase the coupling parameter K, at a certain value $K_c^*(M,L)$ that depends on the size L,M of channels, different squares become ordered. In correspondence of this second (rounded) transition, the magnetization tends to unity and the magnetic susceptibility of the system reaches its maximum value.

C. 2D arrays of squares

Now, we consider a 2D array of a linear size $\mathcal{N}$ consisting of $\mathcal{N}^2$ squares of size L_0 connected by strips (channels) of the length L and the width M as shown in Fig. 11, where we also indicate the lines along which we compute the spin-spin correlation functions. In Fig. 12 we plot the thermodynamic quantities for this system as a function of K for several values of the channel width M. For the 2D array we observe a qualitatively similar scenario as for the 1D array, i.e., the behavior of both the energy density and the heat capacity closely follows that for a single square, whereas the inflection point of the magnetization and the peak in the magnetic susceptibility are shifted to larger values of K; the length of this shift is controlled by the channel width M. A significative difference between 1D and 2D systems is that the latter exhibit a true ordering transition in the thermodynamic limit. This means that the maximum in the susceptibility grows to infinity upon increasing the size of the 2D array, while for 1D arrays this is not the case. A shoulder in the magnetic susceptibility is a ghost of the rounded phase transition in the 2D square.

In Fig. 13 we plot the spin-spin correlation function $G(x)$ for the 2D system. In this case, the correlations along the side of the square are weaker than in the central part, but they reach the value of $G(x)$ in the central part at the points of the channel cross section. We observe that above a certain value of K (roughly between 0.55 and 0.56) $G(x)$ does not decay to zero. This is a clear indication of the existence of order in the network. The transition as signaled by the peak of the susceptibility which occurs at $K \approx 0.55$, in agreement with the Fisher-Privman theory.

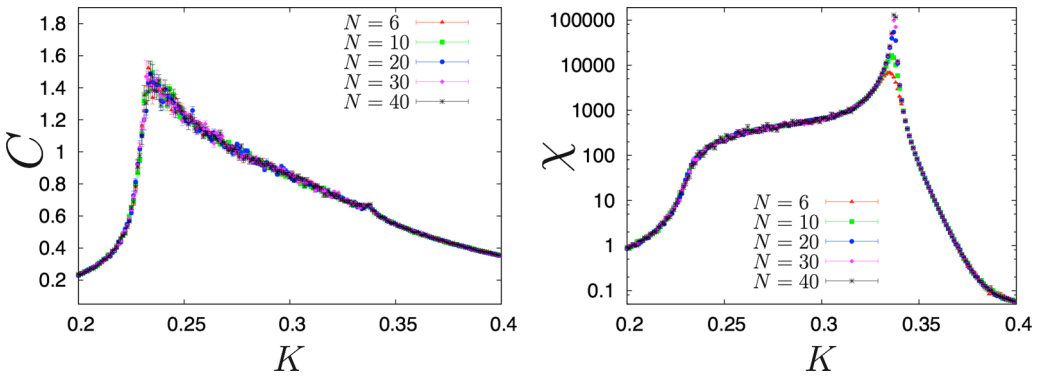

FIG. 15. Thermodynamic quantities for the 2D array of $\mathcal{N} \times \mathcal{N}$ cubes of side $L_0 = 20$ connected (in a periodic way) by channels of size $40 \times 4 \times 4$ as functions of the coupling K: heat capacity C (left panel), magnetic susceptibility χ (right panel).

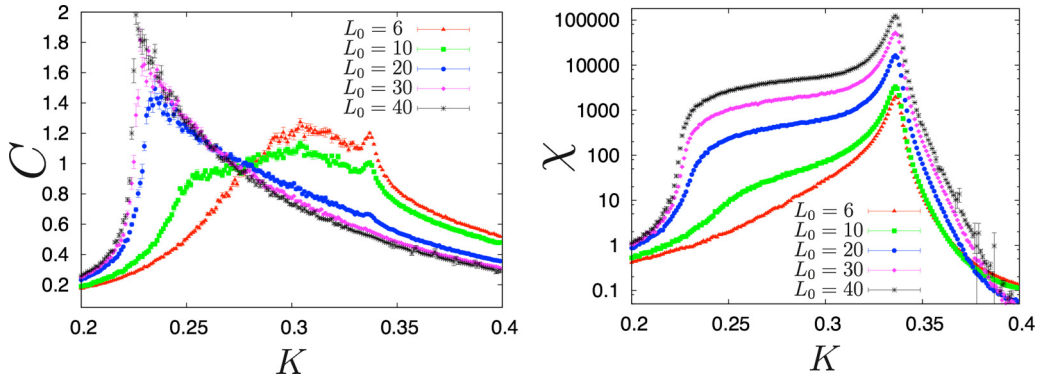

FIG. 16. Thermodynamic quantities for the 2D array of 10×10 cubes of the side L_0 connected (in a periodic way) by channels of size $40 \times 4 \times 4$ as functions of the coupling K: heat capacity C (left panel), magnetic susceptibility χ (right panel).

D. Computation of the effective coupling

We can compute the effective coupling constant between two spin boxes mediated by the channel numerically. Let us consider the strip of the length L and the width M. Along two sides of length L the OBC are applied, whereas two sides of the length M are subjected to the surface fields H_1^- (left side, $x = 1$) and H_1^+ (right size, $x = L$). Further, we assume that the field at the right side is $H_1^+ = +1$ and consider two cases for the field at the left side $H_1^- = -1, +1$. We denote the free energy of the system for these cases F_{++} and F_{-+}, respectively. The surface magnetization at the left side of the strip is $M_1^- = \sum_j \sigma_{1,j}$, whereas at the right side of the strip is $M_1^+ = \sum_j \sigma_{L,j}$. Using the temperature integration method, for $H_1^+ = |H_1^-| = 1$ we can compute free energies:

$$\beta F_{++}(\beta,L,M) = \int_0^\beta \langle E + M_1^- + M_1^+ \rangle_{\beta',L,M} d\beta' \qquad (46)$$

and

$$\beta F_{-+}(\beta,L,M) = \int_0^\beta \langle E + M_1^- - M_1^+ \rangle_{\beta',L,M} d\beta', \qquad (47)$$

where the average $\langle \dots \rangle$ is performed for a given geometry $L \times M$ and inverse temperature β'. The effective interaction constant is thus given by

$$K_{\text{eff}}(\beta,L,M) = \tfrac{1}{2}\beta[F_{-+}(\beta,L,M) - F_{++}(\beta,L,M)]. \qquad (48)$$

Our prediction for the effective interaction constant based on the extended Fisher-Privman theory is given by Eq. (30). In Fig. 14 we plot MC results [Eq. (48)] for $K_{\text{eff}}(\beta,L,M)$ for $L = 100$ and $M = 4,6,10,20,30,40$ as functions of K in comparison with the theoretical results predicted by (30). We observe an excellent agreement between the MC data and the aforementioned theoretical curve.

E. 2D arrays of cubes

In the same way, we have performed various simulations of a 2D 10×10 array of 3D cubes of edges $L_0 = 20$, connected by channels of size $L \times M \times M$ with $L = 40$ and $M = 2,4,6,10,16$. The geometry of the coarse-grained system is exactly the same, as for the 2D system of Fig. 11, but now it consists of 3D cubes and is connected by 3D channels. We have observed that various thermodynamic quantities behave in the same way as for the 2D system. In Fig. 15 we plot both the heat capacity and the susceptibility as functions of the coupling K for $L_0 = 20$ and the channel size $40 \times 4 \times 4$ for various values of the number of cubes $\mathcal{N}$. As expected, the heat capacity does not change by increasing the number of cubes of the network. The magnetic susceptibility exhibits a maximum whose amplitude increases with $\mathcal{N}$, while its location remains

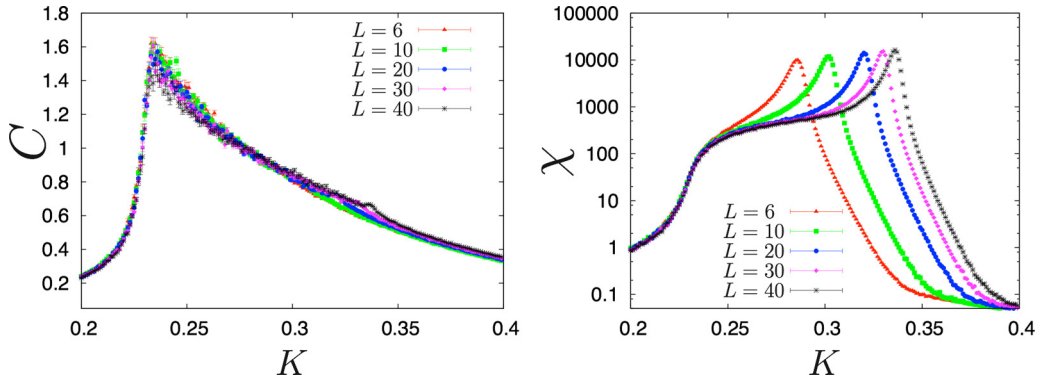

FIG. 17. Thermodynamic quantities for the 2D array of 10×10 cubes of the side $L_0 = 20$ connected (in a periodic way) by channels of the size $L \times 4 \times 4$ as functions of the coupling K: heat capacity C (left panel), magnetic susceptibility χ (right panel).

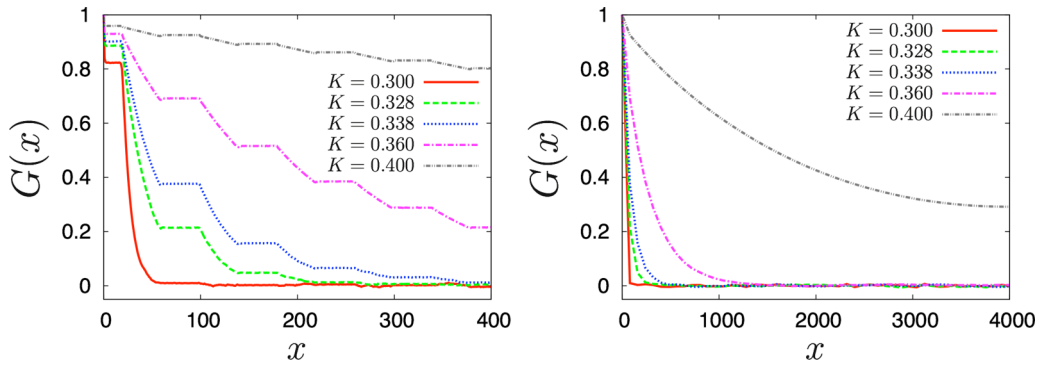

FIG. 18. Left panel: the spin-spin correlation function $G(x)$ as a function of the distance x along the center of the channel [line 1 of Fig. 11(a)], for the 1D array of $\mathcal{N} = 100$ 3D cubes of the linear size $L_0 = 40$ (periodically) connected by channels of the size $40 \times 4 \times 4$ for several values of the coupling K. Right panel: the corresponding values of $G(x)$ at the centers of the cubes.

almost unchanged. We note that contrary to the 2D systems, the heat capacity C exhibits a small peak at the value of K which roughly corresponds to the maximum of the magnetic susceptibility χ.

In Fig. 16 we plot the results for the 2D array of 10×10 cubes connected by channels of the size $40 \times 4 \times 4$ for various cube sizes L_0. For small cubes, $L_0 \leqslant 10$, the heat capacity forms a wide graph with two maxima, a sharp one at $K \simeq 0.34$ (which coincides with the maximum of susceptibility) and a second, broad one. As we increase L_0, the two maxima merge into a single one which gradually increases and shifts toward $K_c \simeq 0.2216$, the critical coupling of the 3D Ising model. The susceptibility has a single pronounced maximum at $K \simeq 0.34$. As we increase L_0, the plateau (shoulder) between this point and K_c is formed. The two-step (or split) transitions in the specific heat shown in Fig. 16 are analogous to the ones illustrated in Fig. 2 of [3], corresponding to exact solutions of the planar Ising model on a strip with a layer of weakened couplings.

In Fig. 17 we plot the thermodynamic quantities for the 2D array 10×10 of cubes of the side $L_0 = 20$ for various channel lengths and fixed cross section equal to 4×4. We observe that the small maximum of the heat capacity changes its position with L in consistence with the behavior of the susceptibility maxima, the latter move toward smaller values of K as the channel length L is increased.

Finally, we have computed the spin-spin correlation function $G(x)$ for the 1D array of 3D cubes as a function of the distance x along the center of the channel [red solid line in Fig. 8(a)]. Comparing Figs. 9 and 18 we can conjecture that the function $G(x)$ in the 1D array of cubes behaves in the same way as $G(x)$ for the 1D array of squares. The only difference is the range of couplings K for which the correlations spread across the whole system: for the 1D array of 3D cubes this occurs at much smaller values of K (larger temperatures).

V. CONCLUSION

In this paper we have presented in details the theory and the MC simulations which explain how an Ising-type system forming a 2D array of boxes connected by narrow channels can support a long-range order on length scales much larger than the bulk correlation length. We show that for a given temperature and width of the 2D channel there exists a critical length of the latter such that the network of boxes is ordered when the channels do not exceed that critical length. Such a theoretical analysis follows from an effective temperature-dependent coupling constant between the boxes that we determined analytically and tested against numerical simulations. Eventually, we have extracted the phase diagram of the planar network of 2D systems. The observed cooperative effect follows from the existence of an emerging length scale that develops inside the connecting channels and dominates over length scales much larger than the ones of bulk fluctuations. The Fisher-Privman theory plays a crucial role in our thinking; for 2D systems we show how important point tension (the analog of the line tension in two dimensions) is in considerations of the validity of this theory, which we subject to a test using the exactly solvable theory of Ising strips. For the planar network of 3D boxes connected by rods, we have provided only the MC simulation results. The extension of the Fisher-Privman theory to this case is a subject of our future work. The cooperative phenomenon that we have found in our system is analogous to the one observed experimentally in superfluid ^{4}He [1] and is a consequence of phase transitions and critical phenomena in confined geometries. The mechanism for the emerging action-at-a-distance which we have described should work for classical binary liquid mixtures at two-phase bulk coexistence, provided that the surfaces of cells and channels have no preference for any of the two phases.

ACKNOWLEDGMENTS

D.B.A. acknowledges the kind hospitality of Prof. S. Dietrich and the Max Planck Institute for Intelligent Systems for multiple visits while this work was done. A.S. wishes to acknowledge the warm hospitality of the Rudolf Peierls Center for Theoretical Physics (Oxford), where part of this work were done.

APPENDIX A: DOMAIN WALL FREE ENERGY

In this appendix, we carry out the detailed computation of (37), making reference to the lattice configuration depicted in Fig. 6. For the sake of completeness we perform the

desired computation by following two different routes. This twofold calculation is actually very instructive as it highlights interesting mathematical features. The transfer matrix from edge to edge of the strip, i.e., along the cylinder axis will be used.[3] Thus, we have an underlying translational, or cyclic, symmetry. The inter-row transfer matrix is the same as used in Sec. II A [see Eq. (1)]. The intrarow matrix is given by

$$V_2 = \exp\left(K_2 \sum_{m=1}^{M} \sigma_m^x \sigma_{m+1}^x\right), \tag{A1}$$

where $\sigma_{M+1}^x = \sigma_1^x$, as required by the cyclic boundary conditions. The disordered state representing the free boundary, denoted 0, may be taken as the state with all spins down in the z direction. Then, the partition function for the strip is

$$Z = \langle 0|(V_2 V_1)^{N-1} V_2|0\rangle. \tag{A2}$$

The analogous quantity for the modified lattice is given by $Z^\times$ where

$$Z^\times = \langle 0|(V_2^\times V_1)^{N-1} V_2^\times|0\rangle, \tag{A3}$$

the operator V_1 is defined by (1) but notice that we omitted the factor in front of the exponential. The modified V_2 is given by

$$V_2^\times = \exp\left(K_2 \sum_{m=1}^{M-1} \sigma_m^x \sigma_{m+1}^x - K_2 \sigma_M^x \sigma_1^x\right). \tag{A4}$$

The key to evaluating Z and $Z^\times$ is to introduce a symmetrized transfer matrix in each case and then to use the Jordan-Wigner transformation to lattice fermions. Define

$$V' = V_1^{1/2} V_2 V_1^{1/2} \tag{A5}$$

and

$$(V')^\times = V_1^{1/2} V_2^\times V_1^{1/2}. \tag{A6}$$

Then, noting that $V_1|0\rangle = e^{MK_1^*}|0\rangle$, it follows that

$$\frac{Z^\times}{Z} = \frac{\langle 0|[(V')^\times]^N|0\rangle}{\langle 0|[V']^N|0\rangle}. \tag{A7}$$

The Jordan-Wigner transformation is given by (4) and the corresponding commutation relations for the lattice Fermi operators are described in Sec. II A. In terms of lattice fermions, we then show that

$$V_1 = \exp\left[-K_1^*\left(\sum_{m=1}^{M} 2 f_m^\dagger f_m - 1\right)\right], \tag{A8}$$

$$V_2 = \exp\left[K_2 \sum_{m=1}^{M-1} (f_m^\dagger - f_m)(f_{m+1}^\dagger + f_{m+1}) - K_2 P_M (f_M^\dagger - f_M)(f_1^\dagger + f_1)\right], \tag{A9}$$

but for the term P_M in V_2 above, both V_1 and V_2 are exponentials of quadratic forms in fermion operators. Moreover, $[V_1, P_M] = 0$ and $[V_2, P_M] = 0$. Thus, we can project onto the invariant subspaces of P_M and consider

$$V_2(\pm) = \exp\left[K_2 \sum_{m=1}^{M-1} (f_m^\dagger - f_m)(f_{m+1}^\dagger + f_{m+1}) \mp K_2 (f_M^\dagger - f_M)(f_1^\dagger + f_1)\right], \tag{A10}$$

and $V'(\pm) = V_1^{1/2} V_2(\pm) V_1^{1/2}$. Then, using $P_M|0\rangle = |0\rangle$ the required ratio of partition functions becomes

$$\frac{Z^\times}{Z} = \frac{\langle 0|[V'(-)]^N|0\rangle}{\langle 0|[V'(+)]^N|0\rangle}. \tag{A11}$$

The evaluation of (A11) can be carried out with the technique of [10], where one uses lattice Fourier transformation

$$F(k) = M^{-1/2} \sum_{m=1}^{M} e^{-ikm} f_m, \tag{A12}$$

with momenta k restricted in two different sets depending on $e^{ikM} = \mp 1$. Consideration of the translational symmetry of the original lattice Pauli spin operators makes the occurrence of these curious periodic and antiperiodic momenta reasonable. Then, by bringing in the pairing ideas of Nambu [14] and of Anderson [13], the above quotient can be evaluated as a ratio of products

$$\frac{Z^\times}{Z} = \prod_{j=1}^{M} \left\{\frac{g_N[(2j-1)\pi/M]}{g_N[2(j-1)\pi/M]}\right\}^{1/2}, \tag{A13}$$

with the 2π-periodic function $g_N(k)$ defined by

$$g_N(k) = \cosh N\gamma(k) + \sinh N\gamma(k) \cos\delta'(k). \tag{A14}$$

The detailed derivation of (A13) from (A11) is not reported here but it can be carried out using the formalism developed in Ref. [29]. The functions γ, δ', and δ^* were introduced by Onsager as elements of a hyperbolic triangle in the Beltrami-Poincaré unit disk version of non-Euclidean geometry:

$$\begin{aligned}
\cosh\gamma(k) &= \cosh 2K_1^* \cosh 2K_2 - \sinh 2K_1^* \sinh 2K_2 \cos k,\\
\cosh 2K_1^* &= \cosh 2K_2 \cosh\gamma(k) - \sinh 2K_2 \sinh\gamma(k) \cos\delta^*(k),\\
\cosh 2K_2 &= \cosh 2K_1^* \cosh\gamma(k) - \sinh 2K_1^* \sinh\gamma(k) \cos\delta'(k).
\end{aligned} \tag{A15}$$

These are the hyperbolic cosine formulas for the Onsager hyperbolic triangle [16], which should be supplemented by the hyperbolic sine formulas

$$\frac{\sin\delta^*(k)}{\sin 2K_1^*} = \frac{\sin\delta'(k)}{\sin 2K_2} = \frac{\sin k}{\sinh\gamma(k)}. \tag{A16}$$

These formulas are extremely useful for simplifying expressions, as should become apparent. The evaluation of the ratio of products may be made by first exponentiating (A13): then

[3] In this appendix M denotes the length of the horizontal edge and N the strip width; this notation is due to historical reasons. The final results are obviously covariant under the mutual exchange of K_1 with K_2.

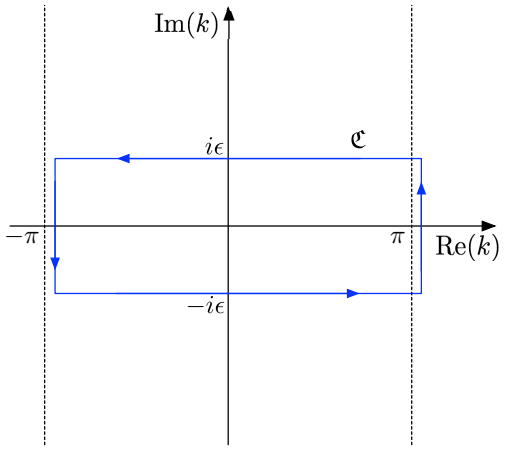

FIG. 19. The integration contour $\mathfrak{E}$ in the complex k plane. The vertical lines have $\mathrm{Re}(k) = \pi[1 + 1/(4M)]$ and $\mathrm{Re}(k) = -\pi[1 - 1/(4M)]$, so that they pass between zeros of $e^{ikM} = \pm 1$, and π is inside the contour, but not $-\pi$. Note that $g_N(k)$ is even in k and there is 2π periodicity. Thus, the side line contributions cancel.

we have

$$\frac{Z^\times}{Z} = \exp\left[\frac{1}{2}\sum_{j=1}^{M}\{\ln g_N[(2j-1)\pi/M] - \ln g_N[2(j-1)\pi/M]\}\right]. \tag{A17}$$

In order to use summation kernels to evaluate this difference as a contour integral, we need the analytic properties of $g_N(k)$ and, of course, its zeros and poles. The branch cuts from $\sinh\gamma(k)$ in (A14) do not contribute. Evidently, for $k \in \mathbb{R}$, $g_N(k) > 0$ and, moreover, this property extends to an interval $|\mathrm{Im}(k)| < \epsilon$, $\epsilon < \hat{\gamma}(0)$ where $\hat{\gamma}$ is defined by analogy with γ but with K_1 and K_2 interchanged. Then, we can write

$$\frac{Z^\times}{Z} = \exp\left[\frac{1}{2}\frac{1}{2\pi i}\oint_{\mathfrak{E}} dk\, iM \times\left(\frac{1}{e^{ikM}-1} + \frac{1}{e^{ikM}+1}\right)\ln g_N(k)\right], \tag{A18}$$

where the contour $\mathfrak{E}$ is shown in Fig. 19.

Simplifying this gives

$$\frac{Z^\times}{Z} = \exp\left[\frac{M}{4\pi i}\oint_{\mathfrak{E}} dk\,\frac{1}{\sin Mk}\ln g_N(k)\right]. \tag{A19}$$

Using the even character of $\ln g_N(k)$, this may be written as

$$\frac{Z^\times}{Z} = \exp\left[\frac{M}{\pi}\int_{-\pi+i\epsilon}^{\pi+i\epsilon} dk\,\frac{e^{iMk}}{1-e^{2iMk}}\ln g_N(k)\right]; \tag{A20}$$

we now expand the integrand using the geometric series, reorder summation, and integration by standard theorems to get

$$\frac{Z^\times}{Z} = \exp\left[\sum_{j=0}^{\infty}\frac{M}{\pi}\int_{-\pi+i\epsilon}^{\pi+i\epsilon} dk\, e^{i(2j+1)Mk}\ln g_N(k)\right]. \tag{A21}$$

Now, integrate by parts

$$\frac{Z^\times}{Z} = \exp\left[-\sum_{j=0}^{\infty}\frac{1}{2j+1}\frac{1}{\pi i}\int_{-\pi+i\epsilon}^{\pi+i\epsilon} dk\, e^{i(2j+1)Mk}\,\frac{g_N'(k)}{g_N(k)}\right]. \tag{A22}$$

The remaining part of the evaluation is to find the zeros of $g_N(k)$. Introducing the conformal transformation $k = i\hat{\gamma}(u)$ rather conveniently does this since

$$g_N[i\hat{\gamma}(u)] = \cos Nu + \frac{\sin Nu}{\sin u}\frac{\cosh 2K_1^*\cos u - \cosh 2K_2}{\sinh 2K_1^*}. \tag{A23}$$

The problem of evaluating zeros of $g_M[\hat{\gamma}(u)]$ can then be reduced to finding the solutions of

$$e^{2iNu} = e^{2i\widehat{\delta^*}(u)}, \tag{A24}$$

where the angle $\widehat{\delta^*}$ is derived from δ^* by interchanging K_1 and K_2. Of particular interest is the subcritical region. If $N < \kappa$, with $\kappa \equiv d\widehat{\delta^*}(\omega)/d\omega|_{\omega=0}$, there are N real solutions u_j, $j = 1,\ldots,N$, such that for each such j there is a solution in the open interval $(\pi(j-1)/N, \pi j/N)$. We now select the zeros of $g_N(k)$ in the upper half plane, and get

$$\frac{Z^\times}{Z} = \exp\left[-\sum_{\ell=1}^{N}\sum_{j=0}^{\infty}\frac{2}{2j+1}e^{-(2j+1)M\hat{\gamma}(u_\ell)}\right], \tag{A25}$$

the sum can be identified and carried out explicitly, giving

$$\frac{Z^\times}{Z} = \prod_{\ell=1}^{N}\tanh\left[\frac{M\hat{\gamma}(u_\ell)}{2}\right]. \tag{A26}$$

On the other hand, if $N > \kappa$ and, of course $K_1^* < K_2$ there is a single imaginary solution for u in the upper half plane. What is happening is that two solutions $\pm u_1$ for $N > \kappa$ (if u is a solution, then so is $-u$) coalesce at the origin when $N = \kappa$ and then go onto the imaginary axis as $\pm i v_1$, for $N > \kappa$, a bifurcation phenomenon, with

$$\hat{\gamma}(i v_1) = 2\sinh 2K_2^*\sinh\gamma(0)\, e^{-N\gamma(0)} + O(e^{-2N\gamma(0)}). \tag{A27}$$

We then find the asymptotic form (37). The reader who is acquainted with the classical results of [10] would more than likely choose the above method to evaluate the domain wall weight w.

Another derivation follows, one which makes the origin of the product of hyperbolic tangents, the function $\gamma(u)$, and the particular choice of the u_j clearer, that is, one which makes the *physical* origin of the structure more obvious. If we consider transfer along the strip as in Fig. 2, that is, exactly what took us to the formula for the pair correlation function for spins in the edge of a strip, we have

$$\frac{Z^\times}{Z} = \frac{\mathrm{Tr}[(V')^N P_M]}{\mathrm{Tr}[(V')^N]} \tag{A28}$$

and

$$\frac{Z^\times}{Z} = \prod_k \tanh\left[\frac{N\gamma(k)}{2}\right]. \tag{A29}$$

Here, we have

$$V_1 = \exp\left[-K_1^* \sum_{m=1}^{M} (2 f_m^\dagger f_m - 1)\right], \tag{A30}$$

$$V_2 = \exp\left[K_2 \sum_{m=1}^{M-1} (f_m^\dagger - f_m)(f_{m+1}^\dagger + f_{m+1})\right]. \tag{A31}$$

Notice the range of summation in V_2, as required by the free-edged strip. Now, it turns out that symmetrized form V can be diagonalized [8] in the form

$$V = \exp\left\{-\sum_k \gamma(k)[X^\dagger(k)X(k) - 1/2]\right\}. \tag{A32}$$

The $\{X(k), X^\dagger(k)\}$ are Fermi operators with vacuum $|\Phi\rangle$ which therefore satisfies $X(k)|\Phi\rangle = 0$; moreover, $P_M|\Phi\rangle = |\Phi\rangle$. Since we have

$$P_M X^\dagger(k_1)\ldots X^\dagger(k_n)|\Phi\rangle = (-1)^n X^\dagger(k_1)\ldots X^\dagger(k_n)|\Phi\rangle, \tag{A33}$$

and $n_k = X^\dagger(k)X(k)$ is the density operator, it follows that

$$\frac{Z^\times}{Z} = \prod_k \frac{\sum_{n_k=0}^{1}[e^{-[N\gamma(k)+i\pi]n_k}]}{\sum_{n_k=0}^{1}[e^{-N\gamma(k)n_k}]}, \tag{A34}$$

and thus (A29) follows, where the k are given by

$$e^{2iMk} = e^{2i\delta^*(k)}. \tag{A35}$$

This is exactly as we have derived in (37), (38), and (39), provided one remembers to interchange the K_j, $j = 1,2$, and also N and M [compare (A29) and (A26)].

Finally, we show how to prove the positiveness of the point tension. Given that for any subcritical temperature $K_2 < K_1^*$, the surface tension τ of the an interface running along the axis of Fig. 6 obeys the inequality $\tau = \gamma(0) = 2K_2 - 2K_1^* < 2K_2$. Therefore, it follows that $\sinh\tau < \sinh 2K_2$, but since $\sinh 2K_2 \sinh 2K_2^* = 1$, the argument of the logarithm of (39) is strictly positive and less than one, and consequently $\tau_p > 0$.

APPENDIX B: ASYMPTOTIC DEGENERACY

The transfer matrix acting parallel to the strip axis (see Fig. 2) has a unique maximal eigenvector $|\Phi\rangle$ with eigenvalue Λ_0, which is also the vacuum for Fermi creation operators $X(k)$: $X(k)|\Phi\rangle = 0$. For $T < T_c$ and a strip width M satisfying $M > d\delta^*(\omega)/d\omega|_{\omega=0}$, we have a mode with a purely imaginary wave number, excited by the creation operator $X^\dagger(iv)$. Its eigenvalue is $\Lambda_0\, e^{\gamma(iv)}$. So from (A27), it is asymptotically degenerate[4] with $|\Phi\rangle$. Now, $|\Phi\rangle$ is strictly nondegenerate for $M < \infty$. Since $[V, P_M] = 0$, $|\Phi\rangle$ must be simultaneous eigenvector of P_M, so since $P_M^2 = 1$,

$$P_M|\Phi\rangle = \pm|\Phi\rangle. \tag{B1}$$

In fact, $P_M|\Phi\rangle = |\Phi\rangle$. Because $P_M\sigma_1^x P_M = -\sigma_1^x$ we find

$$\langle\Phi|\sigma_1^x|\Phi\rangle = 0. \tag{B2}$$

Thus, there is *never* long-range order in a strip of finite width. Equally well, we have $\langle\Phi|X(iv)\sigma_1^x X^\dagger(iv)|\Phi\rangle = 0$. On examining (22) in the limit $M \to \infty$, we see that the first term no longer decays to zero as $n \to \infty$; in fact, it decays to m_e^2. This is because the emergent length scale in (22), namely, $\xi = e^{M\hat{\gamma}(0)}/[2\sinh\hat{\gamma}(0)\sinh 2K_1^*]$, diverges as $M \to \infty$. The second term becomes an integral and displays a correlation length $1/\gamma(0)$; thus, it vanishes in the "limit" of mesoscale modeling. It is natural to specify putative ordered states (which are *not* eigenstates of V) as

$$|\pm\rangle = 2^{-1/2}[1 \pm X^\dagger(iv)]|\Phi\rangle, \tag{B3}$$

which evidently have the property $P_M|\pm\rangle = |\mp\rangle$. The edge magnetization for $|+\rangle$ is

$$\langle+|\sigma_1^x|+\rangle = \mathrm{Re}\langle\Phi|\sigma_1^x X^\dagger(iv)|\Phi\rangle. \tag{B4}$$

In this connection, there is an analogous formulation for the spontaneous magnetization of the bulk. The evaluation of the associated matrix element in that case is a true *tour de force*, carried out by Yang [30]. The eigenvectors for $k = iv$ are obtained by noting this substitution in (16) and (17). The resulting mode is indeed a surface state in the Fermi lattice language.

[4] We refer the interested reader on the phenomenon of asymptotic degeneracy to [6].

[1] J. K. Perron, M. O. Kimball, K. P. Mooney, and F. M. Gasparini, Coupling and proximity effects in the superfluid transition in ^{4}He dots, Nat. Phys. **6**, 499 (2010).

[2] J. K. Perron and F. M. Gasparini, Giant Coupling Effects in Confined ^{4}He Near T_λ, J. Low. Temp. Phys. **162**, 136 (2011).

[3] M. E. Fisher, Proximity eases confinement, Nat. Phys. **6**, 483 (2010).

[4] J. K. Perron and F. M. Gasparini, Critical Point Coupling and Proximity Effects in ^{4}He at the Superfluid Transition, Phys. Rev. Lett. **109**, 035302 (2012).

[5] D. B. Abraham, A. Maciołek, and O. Vasilyev, Emergent long-range couplings in arrays of fluid cells, Phys. Rev. Lett. **113**, 077204 (2014).

[6] M. Kac, *Mathematical Mechanisms in Phase Transitions, Brandeis Lectures 1966* (Gordon and Breach, New York, 1968).

[7] V. Privman and M. E. Fisher, Finite-size effects at first-order transitions, J. Stat. Phys. **33**, 385 (1983).

[8] D. B. Abraham, On the transfer matrix for the two-dimensional ising model, Stud. Appl. Math. **50**, 71 (1971).

[9] D. B. Abraham, F. Latrémolière, and P. J. Upton, Divergence of the Point Tension at Wetting, Phys. Rev. Lett. **71**, 404 (1993).

[10] T. D. Schultz, D. C. Mattis, and E. H. Lieb, Two-dimensional ising model as a soluble problem of many fermions, Rev. Mod. Phys. **36**, 856 (1964).

[11] B. Kaufman, Crystal statistics. II. Partition function evaluated by spinor analysis, Phys. Rev. **76**, 1232 (1949).

[12] P. Jordan and E. Wigner, Über das paulische äquivalenzverbot, Z. Phys. **47**, 631 (1928).
[13] P. W. Anderson, Random-phase approximation in the theory of superconductivity, Phys. Rev. **112**, 1900 (1958).
[14] H. Bruns and K. Flensburg, *Many-Body Quantum Theory in Condensed Matter Physics* (Oxford University Press, Oxford, 2004), see Sec. 18.5.
[15] J. Bardeen, L. N. Cooper, and J. R. Schrieffer, Theory of superconductivity, Phys. Rev. **108**, 1175 (1957).
[16] L. Onsager, Crystal statistics. I. A two-dimensional model with an order-disorder transition, Phys. Rev. **65**, 117 (1944).
[17] P. D. Lax, *Linear Algebra and Its Applications* 2nd ed. (Wiley, Hoboken, NJ, 2007).
[18] D. B. Abraham and A. Maciołek, Filling Transition: Exact Results for Ising Corners, Phys. Rev. Lett. **89**, 286101 (2002).
[19] D. B. Abraham and A. Maciołek, Exact results for corner filling on a quadratic lattice, Phys. Rev. E **72**, 031601 (2005).
[20] T. T. Wu, Theory of toeplitz determinants and the spin correlations of the two-dimensional ising model. I, Phys. Rev. **149**, 380 (1966).
[21] B. M. McCoy and T. T. Wu, Theory of toeplitz determinants and the spin correlations of the two-dimensional ising model. IV, Phys. Rev. **162**, 436 (1967).
[22] D. B. Abraham, G. Gallavotti, and A. Martin-Löf, Surface tension in the two-dimensional ising model, Physica (Amsterdam) **65**, 73 (1973).
[23] M. E. Fisher and A. E. Ferdinand, Interfacial, Boundary, and Size Effects at Critical Points, Phys. Rev. Lett. **19**, 169 (1967).
[24] B. Widom, Surface Tension of Fluids, in *Phase Transitions and Critical Phenomena*, edited by C. Domb and M. S. Green (Academic, London, 1972), Vol. 2, p. 79.
[25] C. Ruge, P. Zhu, and F. Wagner, Correlation function in Ising models, Phys. A (Amsterdam) **209**, 431 (1994).
[26] D. P. Landau and K. Binder, *A Guide to Monte Carlo Simulations in Statistical Physics* (Cambridge University Press, London, 2005), p. 155.
[27] K. Binder and E. Luijten, Monte Carlo tests of renormalization-group predictions for critical phenomena in Ising models, Phys. Rep. **344**, 179 (2001).
[28] V. Privman, in *Finite Size Scaling and Numerical Simulations of Statistical Systems*, edited by V. Privman (World Scientific, Singapore, 1990), p. 1.
[29] D. B. Abraham and P. Reed, Interface profile of the Ising ferromagnet in two dimensions, Commun. Math. Phys. **49**, 35 (1976).
[30] C. N. Yang, The spontaneous magnetization of a two-dimensional ising model, Phys. Rev. **85**, 808 (1952).